Formulating the Unicycle on the Sphere Path Planning Problem as a Linear Time-Varying System

Federico Thomas and Jaume Franch

***Abstract*—The kinematics, dynamics, and control of a unicycle moving without slipping on a plane has been extensively studied in the literature of nonholonomic mechanical systems. However, since planar motion can be seen as a limiting case of the motion on a sphere, we focus our analysis on the more general spherical case. This paper introduces a novel approach to path planning for a unicycle rolling on a sphere while satisfying the non-slipping constraint. Our method is based on a simple yet effective idea: first, we model the system as a linear time-varying dynamic system. Then, leveraging the fact that certain such systems can be integrated under specific algebraic conditions, we derive a closed-form expression for the control variables. This formulation includes three free parameters, which can be tuned to generate a path connecting any two configurations of the unicycle. Notably, our approach requires no prior knowledge of nonholonomic system analysis, making it accessible to a broader audience.**

***Index terms*— Nonholonomic robots, nonholonomic joints, linear time-varying systems, path planning.**

I. Introduction

THERE are many examples of robotic systems with velocity constraints that cannot be integrated to give constraints expressed solely in terms of configuration variables (see, for example, the monographs [1, 2] and the references therein). The most prominent example among these so-called nonholonomic robots is the kinematic car, which is equivalent to a unicycle moving on a plane [3, 4]. Driving a kinematic car from an initial configuration to a target configuration is a fundamental problem in robotics that has received significant attention. This problem can be seen as a limiting case of steering a unicycle on a sphere, where the sphere's radius tends to infinity. Although this generalization holds theoretical significance on its own, the problem of controlling a unicycle on a sphere —or, equivalently, the motion of a sphere in contact with a freely rotating disk— also has practical relevance in applications involving nonholonomic spherical joints in parallel robots. The idea of using nonholonomic joints in parallel robots was introduced in [5] as a generalization of the nonholonomic wrist proposed in [6], or the parallel mobile robot described in [7]. The analysis in [5] was later corrected and extended in [8, 9]. Further developments can be found in [10, 11, 12, 13]. A possible implementation of such a joint is depicted in Fig. 1. The sphere cannot execute arbitrary spherical motions but can attain any orientation by following an appropriate path. A major drawback of robots using these joints is the complexity of their control. Although simple control strategies can be devised by alternating rotations about the unconstrained axes (the x- and y-axes in Fig. 1) [6], this approach leads to slow movements due to the presence of zero-velocity configurations along the path. A first attempt to generate coordinated motions about the unconstrained axes was presented in [10]. In this paper, we reformulate the problem and provide a complete solution, including a characterization of its singularities.

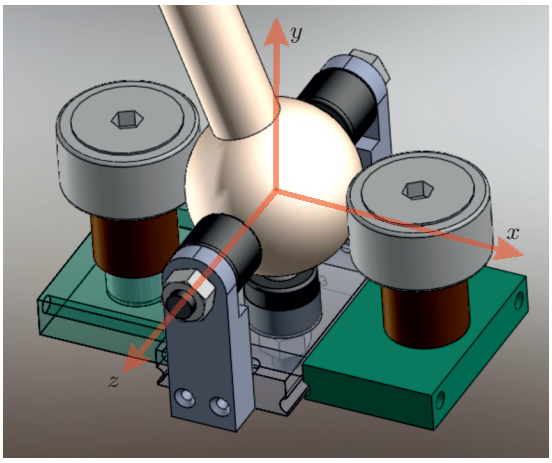

Fig. 1. Nonholonomic spherical joint [13]. While the sphere can freely rotate about the $x-$ and the $y-$axis, its rotation about the $z-$axis is constrained by the two freely rotating disks. By fixing the world reference frame to the sphere rather that the base, the joint's mobility becomes equivalent to that of a monocycle on a sphere.

This paper addresses a point-to-point path planning problem for a unicycle rolling on a sphere, focusing on generating a path that leads the system to a desired final configuration. In control-theoretic terms, this corresponds to a *global* stabilization problem. The term global emphasizes that the target configuration is not necessarily close to the initial one. The solution to this problem must yield a kinematically feasible path, ensuring perfect execution under nominal conditions. A natural first approach is to extend existing methods used for the analogous problem of a kinematic car on a plane. While a comprehensive review of the literature on this topic is beyond the scope of this paper, we provide a brief overview

The authors are with the Institut de Robòtica i Informàtica Industrial (CSIC-UPC), ETSEIB, Diagonal 647, Pavelló E, planta 1, 08028 Barcelona, Spain, and with the Department of Mathematics (UPC), Pau Gargallo 14, 08028 Barcelona, Spain. f.thomas@csic.es, jaume.franch@iri.upc.edu

This paper is dedicated to the memory of our dear colleague and friend Prof. Ettore Penestri.

to contextualize our contribution.

Although intuition suggests that a unicycle —whether on a plane or a sphere— is fully controllable, establishing this property rigorously is nontrivial. A unicycle on a plane has two control inputs (longitudinal velocity and steering angle) to regulate three configuration variables (the Cartesian coordinates of a reference point on the unicycle and its orientation). However, a controllability analysis based on linear approximations is insufficient. In fact, as shown in [14], a necessary condition for controllability cannot be satisfied using a smooth, time-invariant feedback. Consequently, researchers have explored stabilizing controllers based on nonsmooth and/or time-varying feedback control laws. In this context, the identification of canonical forms for kinematic models of nonholonomic robots has been crucial, as these forms facilitate the design of time-varying feedback controllers. The most widely used canonical structure is the *chained form*, which, in the case of a unicycle on a plane, is mathematically equivalent to the *Chaplygin form* and the *power form*. The introduction of differential flatness shifted interest away from these canonical forms. Differential flatness implies the existence of a dynamic state feedback transformation that converts the system into a linear and decoupled structure composed of input-output chains of integrators [15]. When it was proven that the kinematic car model is differentially flat [16, 17], many researchers considered the problem effectively solved, leading to a decline in interest. Other approaches have also yielded significant results [18, 19, 20], but the method based on sinusoidal inputs [21] is particularly relevant to our study, as our solution naturally results in sinusoidal inputs without explicitly enforcing them.

Heuristic and ad hoc approaches have also played a significant role in the development of path planners for car-like robots due to their simplicity. The pioneering work of [22] demonstrated that paths connecting two arbitrary configurations of a car-like robot can be represented as a finite sequence of two elementary components: circular arcs (with minimal turning radius) and straight-line segments. Most practical motion planners for such robots generate paths composed of these elements. As a result, the paths are piecewise C^2, meaning they are C^2 within each elementary segment but exhibit curvature discontinuities at transition points [23]. To navigate these discontinuities, the robot must stop to ensure continuity in linear and angular velocities. To mitigate this issue, a smoothing technique was introduced in [24], allowing the generated paths to be C^2 except at cusp points.

A simple kinematic inversion transforms the path planning problem of a unicycle rolling on a sphere into that of reorienting a sphere using two controls [10]. Interestingly, despite being more general than the planar case, this problem admits a simpler formulation. The key distinction lies in dimensional homogeneity: while the planar case involves both distances and angles, the spherical case depends solely on angles. The significance of the spherical case stems from its connection to the planar case. Specifically, a solution for the spherical case extends naturally to the planar case, as elements of the rigid motion group in $\mathbb{R}^2$, $SE(2)$, can be approximated by elements of the rotation group in $\mathbb{R}^3$, $SO(3)$, in much the same way that elements of $SE(3)$ can be approximated by elements of $SO(4)$ [25]. This perspective introduces a fundamentally new approach to the path planning problem for a unicycle on a sphere. Although the problem of controlling the motion of a unicycle on a sphere can be shown to be differentially flat [26], we found that existing algorithms for computing flat outputs (see, for instance, [27]) lead to a system of partial differential equations that cannot be solved analytically. This limitation motivated our search for an alternative approach, ultimately leading us to formulate the system as a time-varying system that can be integrated.

This paper is organized as follows. In the next section, we review the differential equations governing the motion of a unicycle on a sphere in their standard form. We then demonstrate how a simple shift in the world reference frame significantly simplifies the formulation, allowing it to be expressed as a linear time-varying system. This new formulation introduces three constant matrices, whose properties are analyzed in Section III. The path planning problem is addressed in Section IV. To illustrate and validate the theoretical results, four examples are presented in Section V. Finally, Section VI summarizes the main contributions and highlights open problems that warrant further investigation.

II. Equations of motion

A. Standard approach: moving unicycle

In what follows, we denote the 4×4 identity and zero matrix by $\mathbf{I}$ and $\mathbf{0}$, respectively.

Following the notation used in Fig. 2, the system equation can be expressed as $\mathbf{A}(\mathbf{s})\dot{\mathbf{s}} = 0$. That is,

$$\begin{pmatrix} 1 & 0 & 0 & -\dfrac{r}{R}\dfrac{\cos\gamma}{\cos\psi} \\ 0 & 1 & 0 & -\dfrac{r}{R}\sin\gamma \end{pmatrix} \begin{pmatrix} \dot\theta \\ \dot\psi \\ \dot\gamma \\ \dot\phi \end{pmatrix} = \mathbf{0}, \tag{1}$$

where $\mathbf{s} = (\theta, \psi, \gamma, \phi)^T$ is the state vector (see [28] for details).

Equation (1) is valid almost everywhere, except at the poles where $\psi = \pm\pi/2$. This is an important drawback. Moreover, $\dot\gamma$ should not be interpreted as the angular velocity of the disk on the sphere, which is given by $\dot\chi$. They are actually related through the following expression:

$$\dot\gamma = \dot\chi - \frac{r}{R}\cos\gamma\,\tan\psi\,\dot\phi. \tag{2}$$

The formulation of a unicycle on a plane can be derived as a limiting case of the spherical model. Specifically, as $R \to \infty$, we approximate $\theta \approx x/R\cos\psi$ and $\psi \approx y/R$. Substituting these expressions into (1) yields:

$$\begin{pmatrix} 1 & 0 & 0 & -r\cos\gamma \\ 0 & 1 & 0 & -r\sin\gamma \end{pmatrix} \begin{pmatrix} \dot x \\ \dot y \\ \dot\gamma \\ \dot\phi \end{pmatrix} = \mathbf{0}, \tag{3}$$

where (x, y) denotes the Cartesian position of the robot, and γ denotes the robot's orientation with respect to the x-axis. Furthermore, from (2), we obtain $\dot\gamma = \dot\chi$ in the limit as $R \to \infty$.

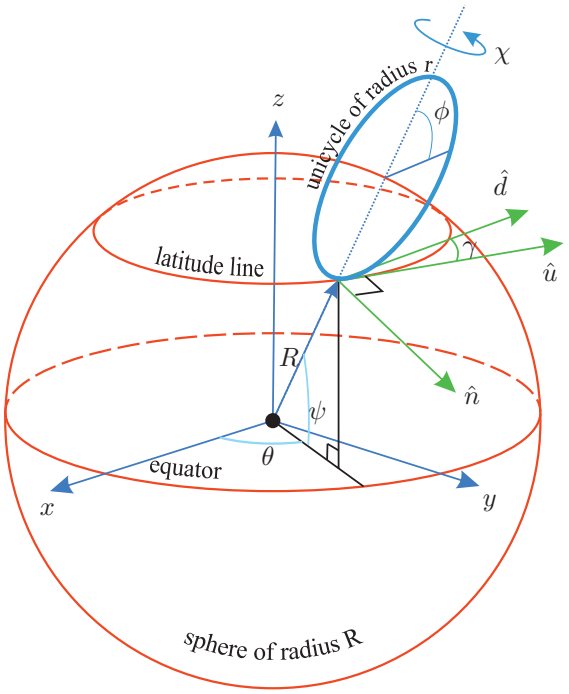

Fig. 2. To characterize the motion of a unicycle on a sphere using the standard formulation, three reference frames are required: one for the sphere, one for the unicycle, and a third with its origin at the point of contact between the sphere and the unicycle. This results in a considerable amount of notation.

By applying the technique of the Lie bracket rank condition, the systems described by (1) and (3) can be shown to be controllable at any point (see [28] for the spherical case and [29] for the planar case). Consequently, in the spherical case, by independently varying the forward velocity $r\dot{\phi}$ and the angular velocity $\dot{\gamma}$, the unicycle can be steered to any target configuration.

Since the system is driftless with four states and two inputs, the controllability of the system implies that it is differentially flat [26]. However, as mentioned in the introduction, computing the flat outputs using existing algorithms results in a system of partial differential equations that cannot be solved analytically.

B. Alternative approach: moving sphere

By fixing the location of the unicycle, we only need to keep the reference frame centered at the sphere which is now the moving object. To avoid representation singularities, the orientation of the sphere can be described using Euler parameters. If we arrange these parameters as the elements of a quaternion, denoted by $\mathbf{q}$, the rate of change of $\mathbf{q}$ is given by the well-known equation (see e.g. [30, p.512] or [31]):

$$\dot{\mathbf{q}} = \frac{1}{2}\begin{pmatrix} 0 & -\omega_x & -\omega_y & -\omega_z \\ \omega_x & 0 & -\omega_z & \omega_y \\ \omega_y & \omega_z & 0 & -\omega_x \\ \omega_z & -\omega_y & \omega_x & 0 \end{pmatrix}\mathbf{q} = \frac{1}{2}\left(\mathbf{A}_x\omega_x + \mathbf{A}_y\omega_y + \mathbf{A}_z\omega_z\right)\mathbf{q}, \tag{4}$$

where the scalar elements correspond to the angular velocity vector components, *i.e.*, $\boldsymbol{\omega} = (\omega_x, \omega_y, \omega_z)$, and

$$\mathbf{A}_x = \begin{pmatrix} 0 & -1 & 0 & 0 \\ 1 & 0 & 0 & 0 \\ 0 & 0 & 0 & -1 \\ 0 & 0 & 1 & 0 \end{pmatrix}, \tag{5}$$

$$\mathbf{A}_y = \begin{pmatrix} 0 & 0 & -1 & 0 \\ 0 & 0 & 0 & 1 \\ 1 & 0 & 0 & 0 \\ 0 & -1 & 0 & 0 \end{pmatrix}, \tag{6}$$

and

$$\mathbf{A}_z = \begin{pmatrix} 0 & 0 & 0 & -1 \\ 0 & 0 & -1 & 0 \\ 0 & 1 & 0 & 0 \\ 1 & 0 & 0 & 0 \end{pmatrix}. \tag{7}$$

Now, analogously to what happens in Fig. 1, we can position the unicycle in such a way that it imposes the constraint ω_z=0. This constraint corresponds to the unicycle's non-slipping condition, but with the sphere considered as the moving object. As a result, the equation of motion of the sphere is reduced to the standard equation of a time-varying linear system $\dot{\mathbf{q}} = \mathbf{A}(t)\mathbf{q}$ with

$$\mathbf{A}(t) = \frac{1}{2}\left(\mathbf{A}_x\omega_x + \mathbf{A}_y\omega_y\right). \tag{8}$$

The resulting simplicity is remarkable when compared to the standard formulation.

Before proceeding further, it is important to examine the properties of the set of matrices given in (5)-(7).

III. Properties of $\{\mathbf{A}_x, \mathbf{A}_y, \mathbf{A}_z\}$

Observe that $\mathbf{A}_x$, $\mathbf{A}_y$, and $\mathbf{A}_z$ are both antisymmetric and orthogonal. In other words, $\mathbf{A} = -\mathbf{A}^T$ and $\mathbf{A}\mathbf{A}^T = \mathbf{I}$. As a consequence,

$$\mathbf{A}_x^2 = \mathbf{A}_y^2 = \mathbf{A}_z^2 = -\mathbf{I}. \tag{9}$$

Moreover, it can be verified that

$$\mathbf{A}_x\mathbf{A}_y\mathbf{A}_z = -\mathbf{I}. \tag{10}$$

Equations (9) and (10) give enough information to derive the following product table

	$\mathbf{I}$	$\mathbf{A}_x$	$\mathbf{A}_y$	$\mathbf{A}_z$
$\mathbf{I}$	$\mathbf{I}$	$\mathbf{A}_x$	$\mathbf{A}_y$	$\mathbf{A}_z$
$\mathbf{A}_x$	$\mathbf{A}_x$	$-\mathbf{I}$	$\mathbf{A}_z$	$\mathbf{A}_y$
$\mathbf{A}_y$	$\mathbf{A}_y$	$-\mathbf{A}_z$	$-\mathbf{I}$	$-\mathbf{A}_x$
$\mathbf{A}_z$	$\mathbf{A}_z$	$\mathbf{A}_y$	$-\mathbf{A}_x$	$-\mathbf{I}$

(11)

This is equivalent to the product table of the real unit and the three imaginary units used to define a quaternion. This is why equations (9) and (10) are referred to as the *Hamiltonian conditions*. In [32], it is demonstrated that there are a total of 48 distinct ordered sets of three 4×4 skew-symmetric matrices and their signed permutations that, together with the identity matrix, can serve as a basis for quaternion algebra. $\{\mathbf{A}_x, \mathbf{A}_y, \mathbf{A}_z\}$ is one of these sets.

Now, let us consider an arbitrary linear combination of the elements of $\{\mathbf{A}_x, \mathbf{A}_y, \mathbf{A}_z\}$. That is,

$$\mathbf{C} = \begin{pmatrix} 0 & -l_1 & -l_2 & -l_3 \\ l_1 & 0 & -l_3 & l_2 \\ l_2 & l_3 & 0 & -l_1 \\ l_3 & -l_2 & l_1 & 0 \end{pmatrix} = l_1\mathbf{A}_x + l_2\mathbf{A}_y + l_3\mathbf{A}_z. \quad (12)$$

Then, it can be verified (see, for example, [33, p. 139]) that

$$e^{\theta\mathbf{C}} = \cos\theta\,\mathbf{I} + \operatorname{sinc}\theta\,\mathbf{C}, \quad (13)$$

where $\operatorname{sinc}\theta = \dfrac{\sin\theta}{\theta}$ (i.e., the standard sinc function).

IV. Path planning

In the 1970s, M.-Y. Wu published a series of papers on the solution, stability, and transformation of a class of linear time-varying systems [34, 35, 36, 37]. Wu's main result states that the solution to the linear time-varying system $\dot{\mathbf{q}} = \mathbf{A}(t)\mathbf{q}$ can be expressed as

$$\mathbf{q}(t) = e^{\mathbf{A}_1 t}e^{\mathbf{A}_2 t}\mathbf{q}(0) \quad (14)$$

if, and only if, there exists a constant matrix $\mathbf{A}_1$ which satisfies

$$\mathbf{A}_1\mathbf{A}(t) - \mathbf{A}(t)\mathbf{A}_1 = \dot{\mathbf{A}}(t), \quad (15)$$

and $\mathbf{A}_2$ is a constant matrix obtained as follows:

$$\mathbf{A}_2 = \mathbf{A}(0) - \mathbf{A}_1. \quad (16)$$

The condition in (15) can only be satisfied by certain time-varying systems. In 1993, Watkins and Yurkovich presented an algorithm to find $\mathbf{A}_1$, if it exists, in their work [38]. However, in our particular problem, the derivation of $\mathbf{A}_1$ can be greatly simplified. In the appendix, we show that the only possible solution must be of the form $\mathbf{A}_1 = k\mathbf{A}_z$, where k is a constant. Thus, we can proceed by taking

$$\mathbf{A}_1 = \frac{\alpha}{2}\mathbf{A}_z \quad (17)$$

where the constant factor have been chosen to be $\frac{\alpha}{2}$ for a neat final result. To verify if (17) is indeed a valid solution, we substitute (8) and (17) into (15). After some algebraic manipulations, we obtain the condition

$$\mathbf{A}_y\alpha\,\omega_x - \mathbf{A}_x\alpha\,\omega_y = \mathbf{A}_x\dot{\omega}_x + \mathbf{A}_y\dot{\omega}_y. \quad (18)$$

From this we conclude that

$$\dot{\omega}_y = \alpha\,\omega_x,$$
$$\dot{\omega}_x = -\alpha\,\omega_y,$$

whose integration leads to

$$\omega_x = a\cos(\alpha t + \alpha_0),$$
$$\omega_y = a\sin(\alpha t + \alpha_0).$$

Therefore, we have

$$\mathbf{A}(t) = \frac{a}{2}\left[\mathbf{A}_x\cos(\alpha t + \alpha_0) + \mathbf{A}_y\sin(\alpha t + \alpha_0)\right], \quad (19)$$

and, consequently,

$$\mathbf{A}_2 = \frac{1}{2}\left(a\cos\alpha_0\mathbf{A}_x + a\sin\alpha_0\mathbf{A}_y - \alpha\mathbf{A}_z\right). \quad (20)$$

Thus, $\mathbf{A}_1$ and $\mathbf{A}_2$, as given in (17) and (20), satisfy (15). Consequently, by properly scaling time, the problem is reduced to finding the constants a, α, and α_0 satisfying the equation

$$\mathbf{q}(1) = e^{\mathbf{A}_1}e^{\mathbf{A}_2}\mathbf{q}(0), \quad (21)$$

or, equivalently,

$$e^{-\mathbf{A}_1}\mathbf{q}(1) = e^{\mathbf{A}_2}\mathbf{q}(0). \quad (22)$$

Hence, using (13), we have that

$$\left(\cos\theta_1\mathbf{I} - \operatorname{sinc}\theta_1\mathbf{A}_1\right)\mathbf{q}(1) = \left(\cos\theta_2\mathbf{I} + \operatorname{sinc}\theta_2\mathbf{A}_2\right)\mathbf{q}(0). \quad (23)$$

where

$$\theta_1 = \frac{1}{2}\alpha \quad \text{and} \quad \theta_2 = \frac{1}{2}\sqrt{a^2 + \alpha^2}. \quad (24)$$

Thus,

$$\alpha = 2\theta_1 \quad \text{and} \quad a = 2\sqrt{\theta_2^2 - \theta_1^2}. \quad (25)$$

Without loss of generality, we can assume that the initial orientation is $\mathbf{q}(0) = (1, 0, 0, 0)$ and the target orientation is $\mathbf{q}(1) = (q_1, q_2, q_3, q_4)$. Substituting the expressions for $\mathbf{A}_1$ and $\mathbf{A}_2$ from (17) and (20) into (23), and expanding the products using the product table in (11), we obtain the following four scalar equations:

$$q_1\cos\theta_1 + q_4\sin\theta_1 = \cos\theta_2, \quad (26)$$
$$q_2\cos\theta_1 + q_3\sin\theta_1 = \sqrt{\theta_2^2 - \theta_1^2}\operatorname{sinc}\theta_2\,\cos\alpha_0, \quad (27)$$
$$q_3\cos\theta_1 - q_2\sin\theta_1 = \sqrt{\theta_2^2 - \theta_1^2}\operatorname{sinc}\theta_2\,\sin\alpha_0, \quad (28)$$
$$q_4\cos\theta_1 - q_1\sin\theta_1 = -\theta_1\operatorname{sinc}\theta_2. \quad (29)$$

These four equations in three unknowns (θ_1, θ_2, and α_0) are not independent because $q_1^2 + q_2^2 + q_3^2 + q_4^2 = 1$.

Notice that α_0 and θ_2 can be readily expressed as a function of θ_1 as follows:

$$\alpha_0 = \operatorname{atan2}\left(q_3\cos\theta_1 - q_2\sin\theta_1, q_2\cos\theta_1 + q_3\sin\theta_1\right), \quad (30)$$
$$\theta_2 = \arccos\left(q_1\cos\theta_1 + q_4\sin\theta_1\right). \quad (31)$$

Moreover, from equation (29), we have that

$$\theta_2 = \theta_1\frac{\sin\theta_2}{q_1\sin\theta_1 - q_4\cos\theta_1}. \quad (32)$$

Then, since $\sin(\arccos x) = +\sqrt{1 - x^2}$, it follows that

$$\theta_2 = \theta_1\frac{\sqrt{1 - (q_1\cos\theta_1 + q_4\sin\theta_1)^2}}{q_1\sin\theta_1 - q_4\cos\theta_1}. \quad (33)$$

By equating the right hand sides of (31) and (33) and rearranging terms, we conclude that

$$\theta_1 = \frac{q_1\sin\theta_1 - q_4\cos\theta_1}{\sqrt{1 - (q_1\cos\theta_1 + q_4\sin\theta_1)^2}}\arccos\left(q_1\cos\theta_1 + q_4\sin\theta_1\right),$$

which can be rewritten as

$$\theta_1 = g'(\theta_1)g(\theta_1) = \frac{1}{2}[g^2(\theta_1)]', \quad (34)$$

where the prime symbol denotes the derivative with respect to θ_1, and

$$g(\theta_1) = \arccos\left(q_1\cos\theta_1 + q_4\sin\theta_1\right)$$
$$= \arccos\left(\upsilon\cos\left(\theta_1 + \xi\right)\right), \quad (35)$$

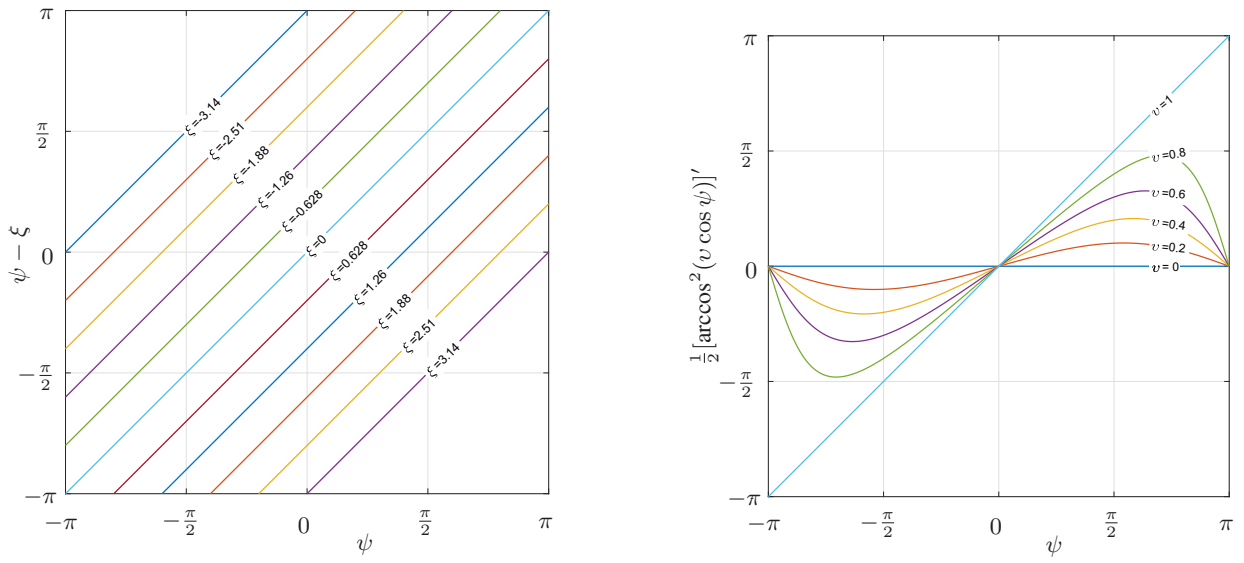

Fig. 3. Graphical analysis of equation (38). Left: plot of its lhs as a function of ψ (with $\xi \in [-\pi, \pi]$ as parameter). Right: plot of its rhs as a function of υ (with $\upsilon \in [-1, 1]$ as parameter). Given values for ξ and υ, the corresponding value of ψ is obtained by computing the intersection of the respective curves. The solution is unique except when $\upsilon = 0$, which introduces a singularity requiring special treatment (see Example II).

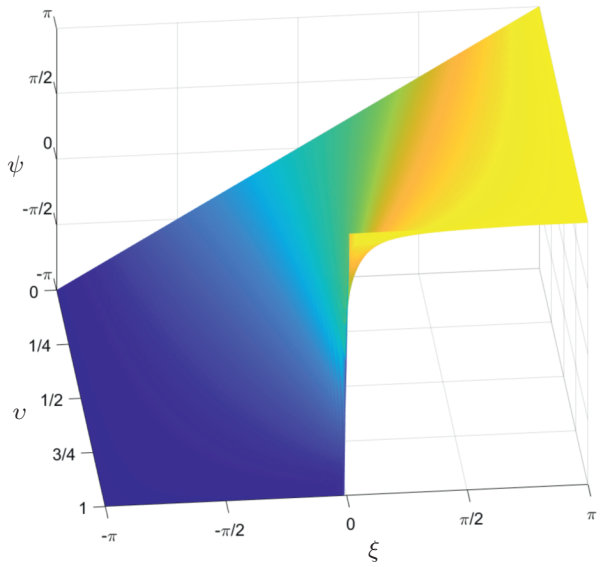

Fig. 4. The values of ψ as a function of υ and ξ can be computed numerically. As υ approaches 1 from the left ($\upsilon \to 1^-$), $\psi(\upsilon, \xi)$ converges to a step function. However, $\psi(1, \xi)$ remains undefined.

with

$$\upsilon = \sqrt{q_1^2 + q_4^2} \in [0, 1] \tag{36}$$

and

$$\xi = \text{atan2}(q_1, q_4) \in [-\pi, \pi]\,. \tag{37}$$

Using the change of variable $\psi = \theta_1 + \xi$, we finally obtain:

$$\psi - \xi = \frac{1}{2}[\arccos^2(\upsilon \cos \psi)]'. \tag{38}$$

Since solving (38) for ψ in closed-form using simple functions appears impossible, a numerical approach is used. To this end, first observe that, while the right-hand side (rhs) of (38) depends on υ, its left-hand side (lhs) depends on ξ. Thus we can plot the lhs of (38) as a function of ψ, treating ξ as a parameter. Similarly, we can plot the rhs as a function of ψ, with υ as a parameter. The resulting plots are shown in Fig. 3. Excluding the case where $\upsilon = 1$, any curve in Fig. 3 (left) intersects with any curve in Fig. 3 (right) at a single point. This implies that a unique solution exists for ψ, except at the singular case where $\upsilon = 1$. Although the function $\psi(\upsilon, \xi)$ cannot be expressed in terms of simple functions, ψ can be obtained through interpolation over a sufficiently dense mesh of points in the (υ, ξ) plane, as illustrated in Fig. 4.

The relevance of the above theoretical findings is better appreciated through the following examples.

V. Examples

A. Example 1: Paths generated for a generic case

Let us consider driving the sphere from its initial orientation $\mathbf{q}(0) = (1, 0, 0, 0)$ to the target orientation specified by

$$\mathbf{q}(1) = (0.8695, 0.2037, 0.3039, -0.3319). \tag{39}$$

For this orientation, (36) and (37) yield $\upsilon = 0.9307$ and $\xi = -0.3646$, respectively. Equation (38) is satisfied for $\psi = 0.7541\pi$ [see Fig. 5(left)]. Consequently, $\theta_1 = \psi - \xi = 2.0043$ and, from (31), $\theta_2 = 2.3002$. Substituting these values of θ_1 and θ_2 into (30) and (25), gives:

$$\alpha_0 = -1.0240, \quad \alpha = 4.0087, \quad a = 2.2571. \tag{40}$$

These parameters, when substituted into (17) and (20), lead to

$$\mathbf{A}_1 = \begin{pmatrix} 0 & 0 & 0 & -2.0043 \\ 0 & 0 & -2.0043 & 0 \\ 0 & 2.0043 & 0 & 0 \\ 2.0043 & 0 & 0 & 0 \end{pmatrix} \tag{41}$$

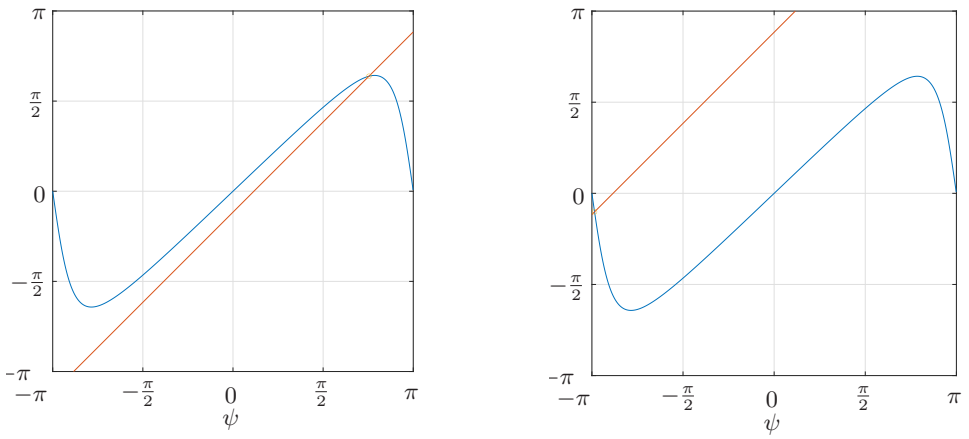

Fig. 5. Plots of the lhs (red) and rhs (blue) of the expression in (38) for $\mathbf{q}(1) = (0.8695, 0.2037, 0.3039, -0.3319)$ (left) and $\mathbf{q}(1) = (-0.8695, -0.2037, -0.3039, 0.3319)$ (right).

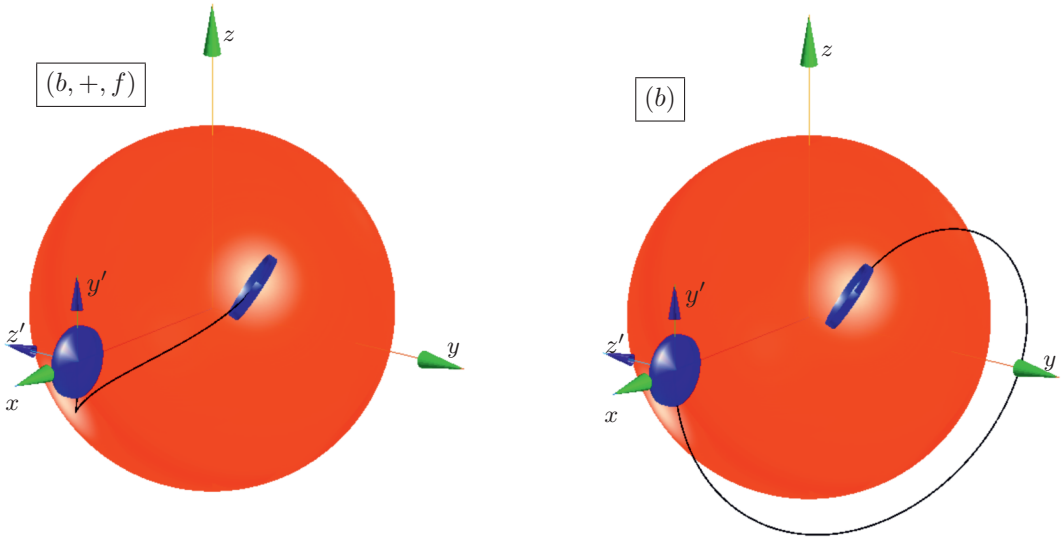

Fig. 6. Path connecting the configuration $\mathbf{q}(0) = (1, 0, 0, 0)$ to $\mathbf{q}(1) = (0.8695, 0.2037, 0.3039, -0.3319)$ (left), and to $\mathbf{q}(1) = (-0.8695, -0.2037, -0.3039, 0.3319)$ (right). These paths are represented after the kinematic inversion that keeps the sphere fixed. They belong to distinct homotopy classes, which remain invariant under *small* perturbations in the target orientation. While this holds for all generic configurations, the behavior changes dramatically at singular configurations.

and

$$\mathbf{A}_2 = \begin{pmatrix} 0 & -0.5868 & 0.9640 & 2.0043 \\ 0.5868 & 0 & 2.0043 & -0.9640 \\ -0.9640 & -2.0043 & 0 & -0.5868 \\ -2.0043 & 0.9640 & 0.5868 & 0 \end{pmatrix}, \qquad (42)$$

respectively.

Finally, the sphere's path to the target orientation, while satisfying the non-slipping constraint $\omega_z = 0$, is given by the time-parameterized solution:

$$\mathbf{q}(t) = e^{t\mathbf{A}_1} e^{t\mathbf{A}_2} \mathbf{q}(0), \quad t \in [0, 1]. \qquad (43)$$

Since our objective is to control the unicycle's motion relative to the sphere, we must apply a kinematic inversion. The result of this transformation is illustrated in Fig. 6(left).

Euler parameters provide a double covering of $SO(3)$, meaning that a unit quaternion $\mathbf{q}$ and its negative $-\mathbf{q}$ represent the same orientation. This motivates us to also consider the antipodal configuration of (39), *i.e.*, $\mathbf{q}(1)=(-0.8695, -0.2037, -0.3039, 0.3319)$. For this case, ξ=2.7769 and υ=0.9307. Then, $\psi = -3.0959$ [see Fig. 5(right)] and, proceeding as above, we have that $\theta_1 = -0.3189$ and θ_2=2.7645. The resulting path of the unicycle's center —after kinematic inversion— is shown in Fig. 6(right). Although both paths connect identical initial and final configurations, they belong to distinct *path homotopy classes*. Paths are central subjects of study in the branch of algebraic topology called homotopy theory. A homotopy of paths makes precise the notion of continuously deforming a path while keeping its endpoints fixed.

In our mechanical system, any admissible path can be decomposed into smooth sub-paths connected by cusps. These components can be classified as follows:

- A *subpath* will be *forward* (f) or *backwards* (b) depending on the sense of motion of the unicycle towards the target.

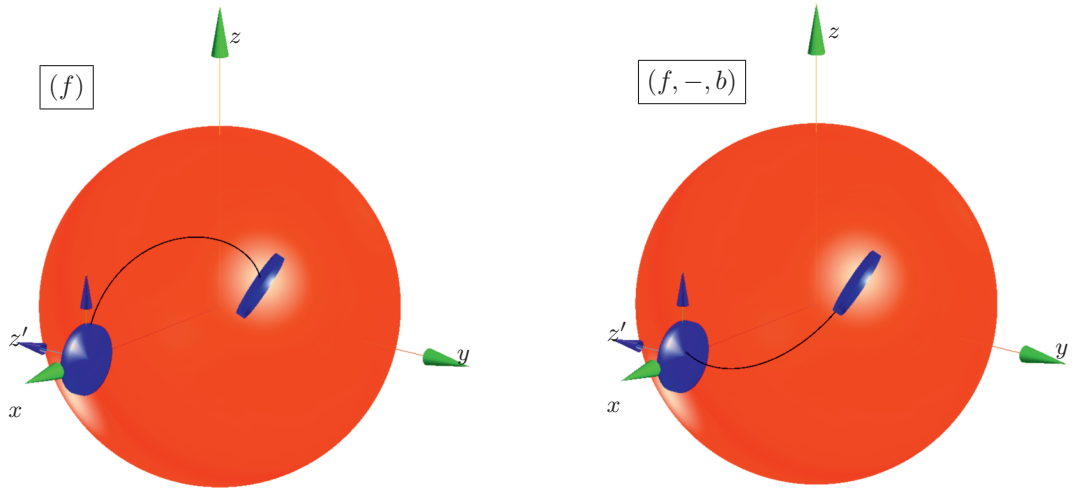

Fig. 7. Path connecting the configuration $\mathbf{q}(0) = (1,0,0,0)$ to $\mathbf{q}(1) = (-0.2037, 0.8695, 0.3319, 0.3039)$ (left), and to $\mathbf{q}(1) = (0.2037, -0.8695, -0.3319, -0.3039)$ (right).

If the path implies a positive rotation about the unicycle z'-axis, we will say that it is a forward path (backwards otherwise).

- A cusp will be *positive* (+) or *negative* (-) depending on the angle formed by the incoming and the outcoming subpaths it connects. If this angle is positive, taken as the angle rotated about an axis perpendicular to the sphere at the point of contact with the unicycle, the cusp will be said to be positive (negative otherwise).

Following this classification scheme, the paths shown in Fig. 6 are characterized by the sequences $(b,+,f)$ and (b), respectively. Under small perturbations of the target configuration (either the original (39) or its negated counterpart), the resulting path deforms continuously while maintaining its homotopy class. However, the situation becomes much more interesting in a singularity, which is analyzed in detail in Section V-B.

To conclude this example, we observe an important symmetry consideration: due to the disk's rotational symmetry about its x-axis, the target configuration $\mathbf{q}(1)$ could be considered as kinematically equivalent to $(0,1,0,0) * \mathbf{q}(1)$, where $*$ denotes quaternion product. The resulting paths, after applying this transformation to our current example, are shown in Fig. 7.

B. Example 2: Paths generated for a singularity

Consider steering the sphere from its initial orientation $\mathbf{q}(0) = (1,0,0,0)$ to the target orientation $\mathbf{q}(1) = (\cos\frac{\pi}{4}, 0, 0, -\sin\frac{\pi}{4})$. For this target orientation, we find that $\upsilon = 1$ and $\xi = -0.7854$. Substituting these values into (38) yields a singularity where no solution exists for ψ. This scenario requires a special handling. Specifically, in this case, equations (27) and (28) are satisfied only when $\operatorname{sinc}\theta_2 = 0$, which occurs if $\theta_2 = n\pi$, $n \in \mathbb{Z}\backslash\{0\}$. Furthermore, α_0 can take any real value, implying that there are infinitely many solution paths, each corresponding to a different value of α_0. The remaining equations, (26) and (29), simplify to a linear system of the form:

$$\begin{pmatrix} \cos\theta_1 & \sin\theta_1 \\ -\sin\theta_1 & \cos\theta_1 \end{pmatrix} \begin{pmatrix} q_1 \\ q_4 \end{pmatrix} = \begin{pmatrix} -1 \\ 0 \end{pmatrix}, \tag{44}$$

whose solution is $q_1 = -\cos\theta_1$ and $q_4 = -\sin\theta_1$. Therefore,

$$\theta_1 = \operatorname{atan2}(-q_4, -q_1). \tag{45}$$

In this example, we have that $\theta_1 = \operatorname{atan2}\left(\sin\frac{\pi}{4}, -\cos\frac{\pi}{4}\right) = \frac{3}{4}\pi$. From (25), we then find that $\alpha = \frac{3}{2}\pi$ and $a = \sqrt{\frac{7}{4}}\pi$. Therefore, it follows that:

$$\mathbf{A}_1 = \frac{3\pi}{4}\mathbf{A}_z, \tag{46}$$

$$\mathbf{A}_2 = \frac{\sqrt{7}\pi}{4}\cos\alpha_0\,\mathbf{A}_x + \frac{\sqrt{7}\pi}{4}\sin\alpha_0\,\mathbf{A}_y - \frac{3\pi}{4}\mathbf{A}_z. \tag{47}$$

The continuum of paths generated by varying α_0 are represented in Fig. 8(left), demonstrating the one-parameter freedom characteristic of singular configurations. Mirroring our analysis of generic cases, we must also consider the antipodal solution family. The resulting family of paths is illustrated in Fig. 8(right).

The path families shown in Fig. 8 exhibit distinct homotopy classes, with class transitions occurring when cusps coincide with path endpoints. Therefore, a homotopy class transition occurs precisely when the unicycle's linear velocity vanishes at either boundary. Eight different homotopy classes can be thus identified. One path belonging to each class is depicted in Fig. 9, together with its homotopy class and the corresponding value of α_0.

As in the previous example, we now consider paths resulting from incorporating an additional half-turn about the disk's x'-axis. The resulting final configurations are no longer singular. The solution paths, shown in Fig. 10, take the form of semicircular arcs. These characteristic patterns correspond to what what in [28] are called "Hawaian necklaces".

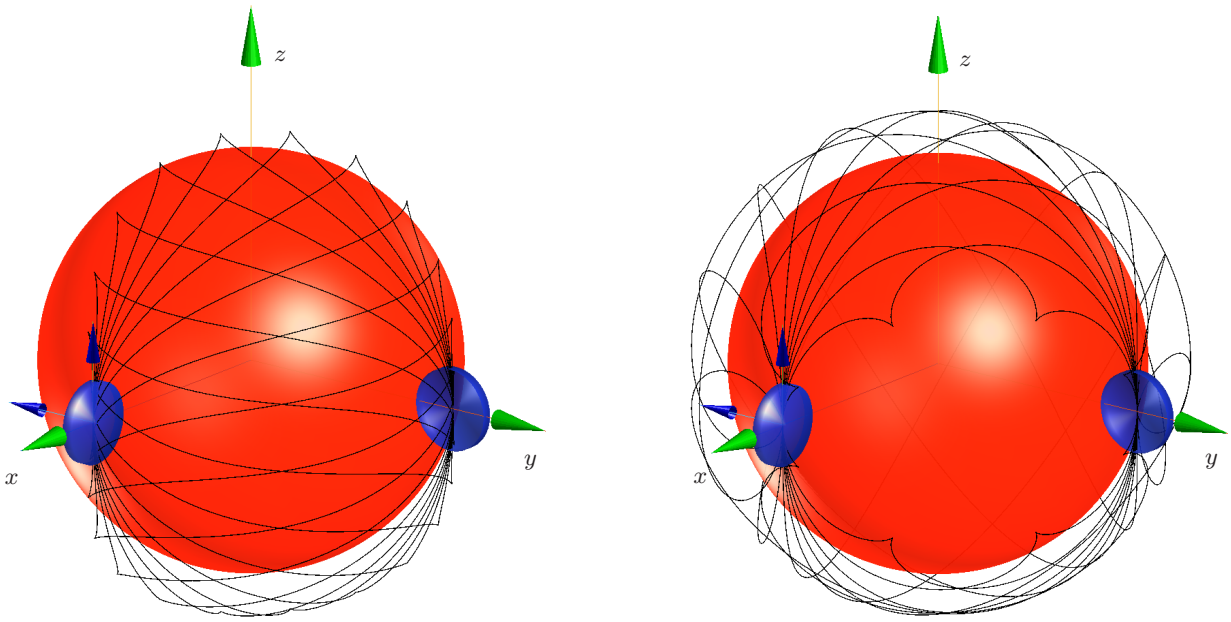

Fig. 8. Paths connecting the sphere's configuration $\mathbf{q}(0) = (1, 0, 0, 0)$ to $\mathbf{q}(1)\left(\cos\frac{\pi}{4}, 0, 0, -\sin\frac{\pi}{4}\right)$ (left), and to $\mathbf{q}(1) = \left(-\cos\frac{\pi}{4}, 0, 0, \sin\frac{\pi}{4}\right)$ (right). They are generated by varying α_0 in the interval $[-\pi, \pi)$.

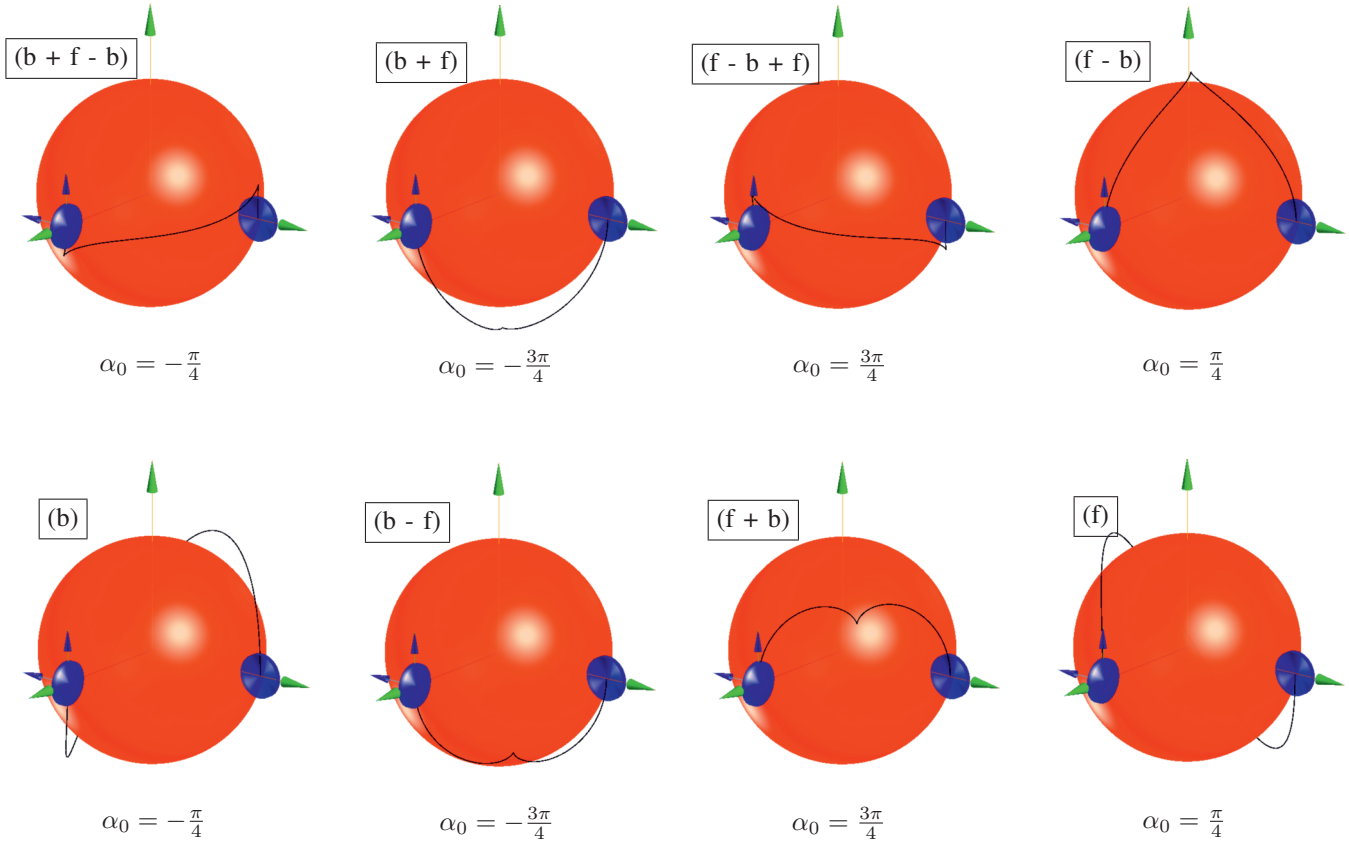

Fig. 9. Paths belonging to different homotopy classes that connect the sphere's configuration $(1, 0, 0, 0)$ to $\left(\cos\frac{\pi}{4}, 0, 0, -\sin\frac{\pi}{4}\right)$ (top row), and $(1, 0, 0, 0)$ to $\left(-\cos\frac{\pi}{4}, 0, 0, \sin\frac{\pi}{4}\right)$ (bottom row).

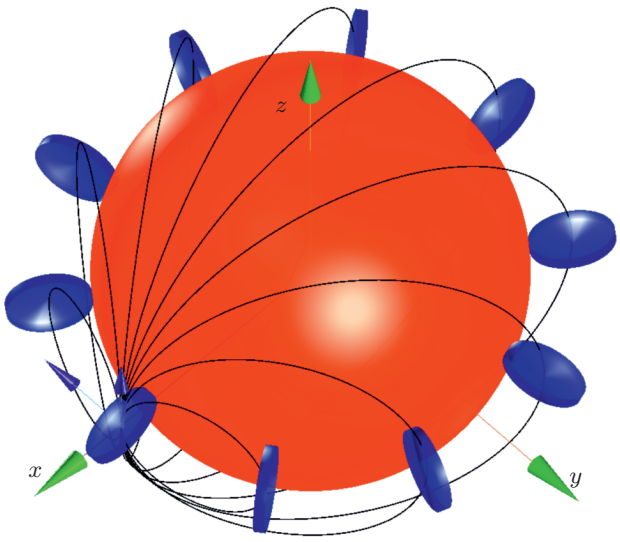

Fig. 10. The so-called "Hawaiian necklaces" originated when connecting the initial configuration $(1,0,0,0)$ to the target configurations $(0,\pm 1,0,0) * (\cos\frac{n\pi}{5}, 0, 0, -\sin\frac{n\pi}{5})$ for $n = \{1,2,\ldots,9\}$.

C. Example 3: Random walks amidst obstacles

In the previous examples, the initial orientation is $\mathbf{q}(0) = (1,0,0,0)$. However, by changing the reference frame, we can start from any arbitrary initial configuration. This flexibility allows us to generate random walks on the sphere by iteratively connecting sequences of randomly chosen orientations. Fig. 11(left) shows a random walk generated from a sequence of 100 uniformly distributed configurations (points in S^3) sampled using the method described in [39]. The same approach can be extended to environments with obstacles. When the disk collides with an obstacle —*e.g.*, one of the seven cylindrical obstacles in Fig. 11(right)—, it stops and attempts to reach the next randomly selected configuration in the sequence.

This example illustrates that the presented path planner can be readily incorporated into broader motion planning frameworks that account for obstacles, such as those described in [40, 41].

D. Example 4: The unicycle on a plane as a limit case

When the unicycle's motion relative to the sphere is constrained to a sufficiently small neighborhood of its initial configuration, its kinematic behavior approximates planar motion. In this case, rotations about the x-axis remain possible, but rotations about the y and z axes must be bounded (see Fig. 12). If these bounds are sufficiently small, the motion of the unicycle relative to the sphere will closely resemble that of a unicycle on a plane. Moreover, recalling that two consecutive rotations about arbitrary axes commute when the rotated angles are *small*, the unicycle will remain within a small region centered at its initial configuration provided that the sphere follows a motion expressed by the quaternion product

$$\mathbf{q}(1) = \left(\cos\frac{\varphi}{2}, \sin\frac{\varphi}{2}, 0, 0\right) * \left(\cos\frac{\delta x}{2D}, 0, 0, \sin\frac{\delta x}{2D}\right) * \left(\cos\frac{\delta y}{2D}, 0, \sin\frac{\delta_y}{2D}, 0\right) \quad (48)$$

$$\approx \left(\cos\frac{\varphi}{2}, \sin\frac{\varphi}{2}, 0, 0\right) * \left(1, 0, \frac{\delta_y}{2D}, \frac{\delta_x}{2D}\right) \quad (49)$$

where D acts as a scaling factor in the translations and is chosen to be sufficiently large so that the errors of the linear approximations of trigonometric functions become negligible. A good lower bound for D comes from the fact that the absolute errors in the computation of $\sin\theta$ and $\cos\theta$, using their linear approximations, remain below $5 \cdot 10^{-5}$ whenever $|\theta| < 0.01$.

As an example, consider a unicycle on a plane, where its configuration is defined by the coordinates of its center (x, y) and its orientation φ. Without loss of generality, we assume that $\varphi = 0$ when the unicycle is parallel to the $\delta y-$axis. Now, suppose we want to drive the unicycle from the initial configuration, given by $(\delta x, \delta y) = (0,0)$ and $\varphi = 0$, to the configurations given by

$$(\delta x, \delta y) = (\cos\psi, \sin\psi), \quad (50)$$

for $\psi = n\,\frac{\pi}{12}$, with $n = 1,\ldots,24$ (*i.e.*, 24 evenly distributed points on the unit circle), and

$$\varphi = \pi, \frac{\pi}{2}, \frac{\pi}{4}, 0. \quad (51)$$

These configurations serve as planar approximations of the spherical motions described by the quaternion product:

$$\mathbf{q}(\varphi,\psi) = \left(\cos\frac{\varphi}{2}, \sin\frac{\varphi}{2}, 0, 0\right) * \left(1, 0, \frac{\sin\psi}{100}, \frac{\cos\psi}{100}\right), \quad (52)$$

where we have chosen $D = 50$. The obtained paths are shown in Fig. 13 for the different values of φ and ψ. Notice how these paths extend far beyond the approximation region as the unicycle's orientation angle approaches 0. For $\varphi = 0$ the obtained paths become impractical, as they circumvent the sphere. To prevent this issue, intermediate configurations with nonzero orientation angles could be introduced to keep the paths within the approximation area. Moreover, when $\varphi = 0$ and $\delta y = 0$, a singularity arises that must be handled separately, as previously discussed.

VI. Conclusion

It is widely accepted that differential geometric methods provide elegant formulations for many problems arising in mechanics, including the path planning problem for car-like robots. In fact, these methods are now considered instrumental in understanding the structural properties of many mechanical systems. However, in this paper, we diverge from this mainstream approach to introduce a novel method for solving the path planning problem of a unicycle rolling on a sphere. The novelty lies in formulating the problem in terms of a time-varying dynamic system whose integration requires no prior knowledge of differential geometry or even nonholonomic systems.

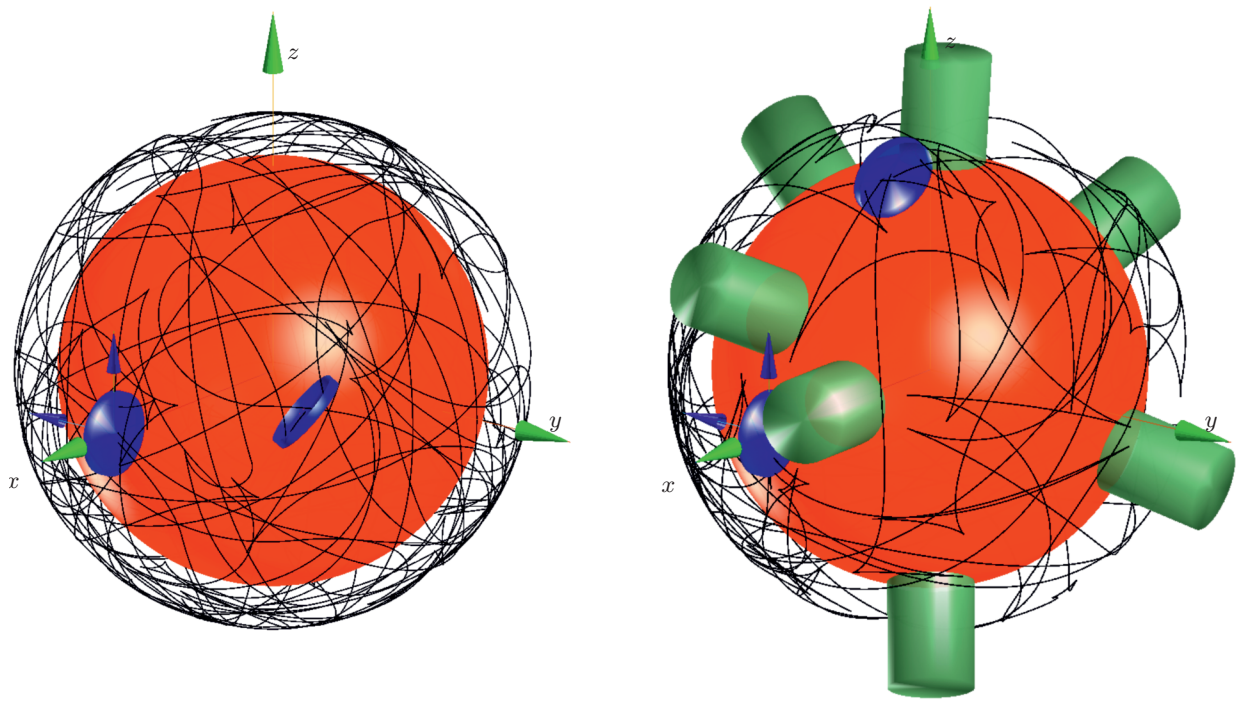

Fig. 11. Ramdom walks without obstacles (left) and with cylindrical obstacles (right). In both cases a sequence of 100 random configurations were used.

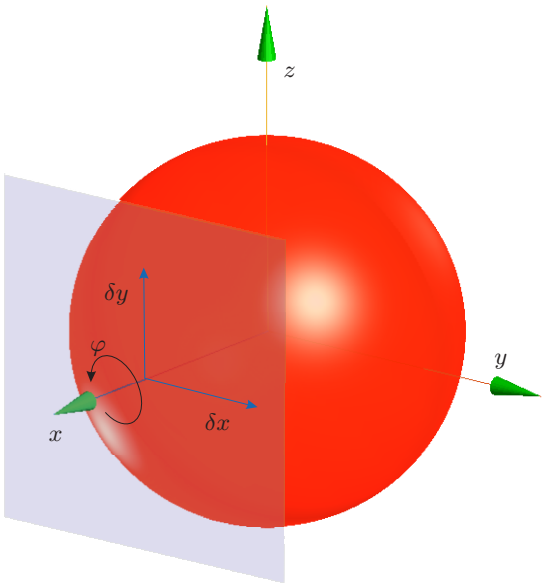

Fig. 12. Planar translations along δx and δy axes can be approximated by rotations in the z and y axes, respectively. The approximation error decreases either increasing the radius of the sphere or, equivalently, scaling down the planar translations.

Finally, it is worth highlighting a couple of points that deserve further attention. First, deriving an approximate closed-form solution to (38) would be valuable. This reduces to finding a bounded-error approximation of the surface in Fig. 4, enabling the proposed method to be integrated into a control loop for path tracking. Second, a detailed differential analysis of the generated curves in S^3 would be useful to determine under what conditions they produce cusps when projected onto S^2. Extending this analysis to obtain the maximum and minimum curvature of a given path could be particularly relevant for integrating the proposed approach into a global motion planner.

ACKNOWLEDGMENTS

We would like to thank Dr. P. Grosch and the anonymous reviewers for their helpful comments. We also gratefully acknowledge the financial support of the Spanish National Plan for Scientific and Technical Research and Innovation through project PID2020-117509GB-I00/MCIN/AEI/10.13039/50110001103

APPENDIX

The value of $\mathbf{A}_1$ satisfying equation (15) can be obtained by using Watkins and Yurkovich's algorithm [38]. However, for our specific problem, we do not need to rely on this algorithm. Instead, by directly substituting (8) into (15) and expanding the result, we can deduce that $\mathbf{A}_1$ must necessarily be a real matrix of the form:

$$\mathbf{A}_1 = \begin{pmatrix} \kappa_1 & \kappa_2 & \kappa_2 & -\kappa_3 \\ -\kappa_2 & \kappa_1 & -\kappa_3 & \kappa_2 \\ -\kappa_2 & \kappa_3 & \kappa_1 & -\kappa_2 \\ \kappa_3 & -\kappa_2 & \kappa_2 & \kappa_1 \end{pmatrix}. \tag{53}$$

Since $\mathbf{A}_1$ must be antisymmetric ($\mathbf{A}_1 = -\mathbf{A}_1^T$), it follows that $\kappa_1 = 0$. Moreover, since it must also be orthogonal ($\mathbf{A}\mathbf{A}^T = \mathbf{I}$), we obtain the conditions $\kappa_2\kappa_3 = 0$ and $2\kappa_2^2 + \kappa_3^2 = 1$. Thus, if we set $\kappa_3 = 0$, then $\kappa_2 = \pm\frac{1}{\sqrt{2}}$. Alternatively, if we set $\kappa_2 = 0$, then $\kappa_3 = 1$. Consequently,

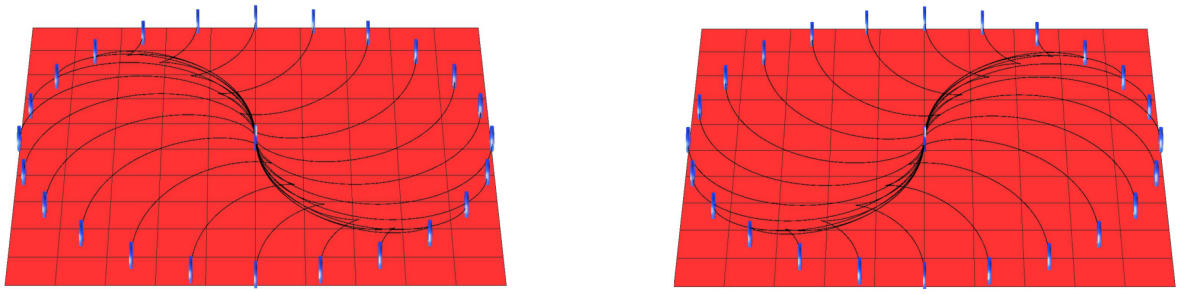

$\varphi = \pi,\ \psi = n\,\frac{\pi}{12},\ n = 1, \ldots, 24.$

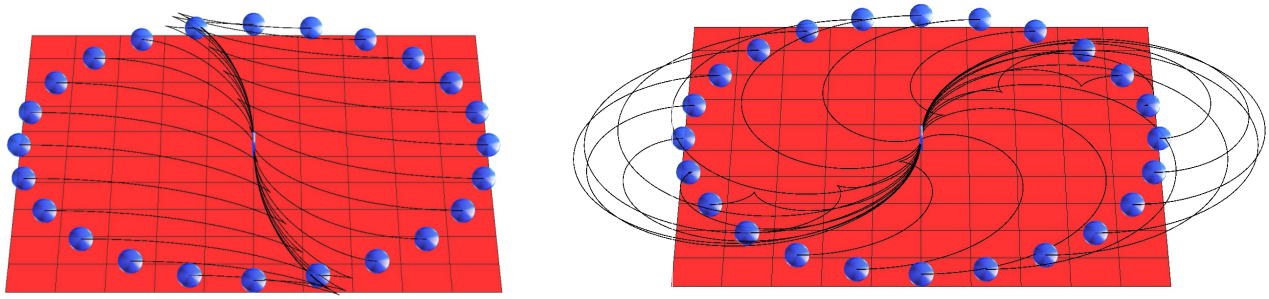

$\varphi = \frac{\pi}{2},\ \psi = n\,\frac{\pi}{12},\ n = 1, \ldots, 24.$

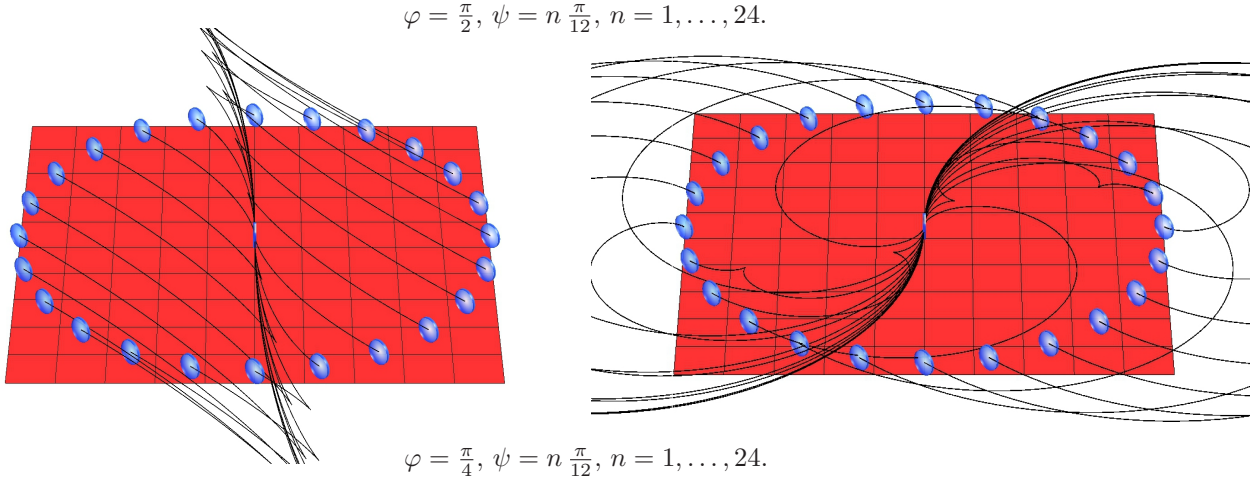

$\varphi = \frac{\pi}{4},\ \psi = n\,\frac{\pi}{12},\ n = 1, \ldots, 24.$

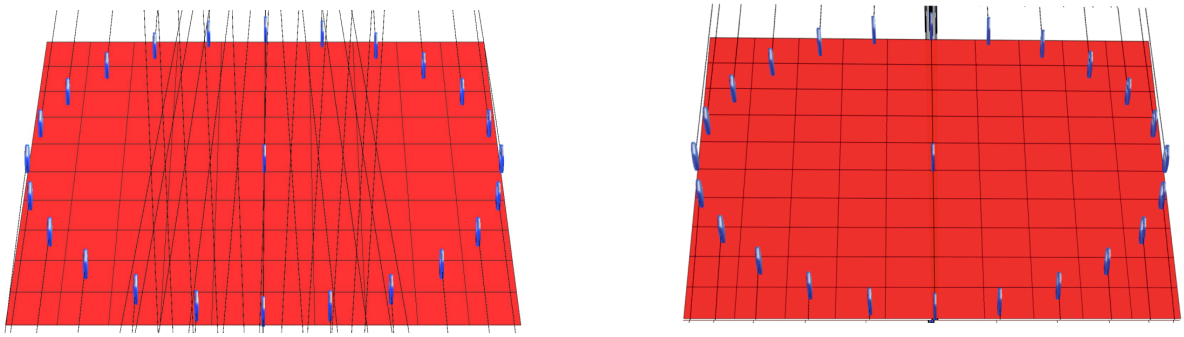

$\varphi = 0,\ \psi = n\,\frac{\pi}{12},\ n = 1, \ldots, 24.$

Fig. 13. Paths families connecting $\mathbf{q}(0) = (1, 0, 0, 0)$ to $\mathbf{q}(1) = \left(\cos\frac{\varphi}{2}, \sin\frac{\varphi}{2}, 0, 0\right) * \left(1, 0, \frac{1}{100}\cos\psi, \frac{1}{100}\sin\psi\right)$ (left column), and to corresponding antipodal configurations (right column). While mathematically describing spherical paths, these trajectories can be regarded, from a practical point of view, as paths followed by a unicycle on a plane.

we have two candidates for $\mathbf{A}_1$, which, up to a scaling constant to be determined, are:

$$\begin{pmatrix} 0 & 1 & 1 & 0 \\ -1 & 0 & 0 & 1 \\ -1 & 0 & 0 & -1 \\ 0 & -1 & 1 & 0 \end{pmatrix} \tag{54}$$

and

$$\begin{pmatrix} 0 & 0 & 0 & -1 \\ 0 & 0 & -1 & 0 \\ 0 & 1 & 0 & 0 \\ 1 & 0 & 0 & 0 \end{pmatrix}, \tag{55}$$

respectively.

Observe that, while (54) coincides with $\mathbf{A}_x + \mathbf{A}_y$, (55) coincides with $\mathbf{A}_z$. To verify whether (54) is a valid solution, we substitute $\mathbf{A}_1 = k(\mathbf{A}_x + \mathbf{A}_y)$, along with (8), into (15). After some algebraic manipulations, we conclude that $\dot{\omega}_x = 0$, $\dot{\omega}_y = 0$, and $\omega_x = -\omega_y$, regardless of the chosen nonzero value of k. Since this solution does not provide sufficient free parameters to compute a path connecting arbitrary orientations, we conclude that, if a valid solution exists, it must necessarily be of the form $\mathbf{A}_1 = k\mathbf{A}_z$.

REFERENCES

[1] B. Lantos and L. Márton, *Nonlinear control of vehicles and robots*, ser. Advances in Industrial Control. London: Springer, 2011.

[2] X. Xin and Y. Liu, *Control design and analysis for underactuated robotic systems*. London: Springer, 2014.

[3] A. De Luca, G. Oriolo, and C. Samson, *Feedback control of a nonholonomic car-like robot*. Berlin: Springer, 1998, vol. 229, pp. 171–253.

[4] C. Collon and J. Rudolph, "Invariant feedback control for the kinematic car on the sphere," *Systems & Control Letters*, vol. 61, no. 10, p. 967–972, 2012.

[5] P. Ben-Horin and F. Thomas, *A Nonholonomic 3-DOF Parallel Robot*. Dordrecht: Springer Netherlands, 2008, pp. 111–118.

[6] C. Stammes, P. Prest, and C. Mobley, "A friction drive robot wrist: electronic and control requirements," *Mechatronics*, vol. 2, no. 4, pp. 391–401, 1992.

[7] S. Shoval and M. Shoham, *Motion Analysis of a Parallel Mobile Robot*. Berlin, Heidelberg: Springer Berlin Heidelberg, 2006, vol. 24, pp. 323–331.

[8] P. Grosch, R. Di Gregorio, and F. Thomas, "Generation of under-actuated parallel robots with non-holonomic joints and kinetostatic analysis of a case study," in *Volume 7: 33rd Mechanisms and Robotics Conference, Parts A and B*. San Diego, California, USA: ASMEDC, 2009, pp. 979–986.

[9] ——, "Generation of under-actuated manipulators with nonholonomic joints from ordinary manipulators," *ASME Journal of Mechanisms and Robotics*, vol. 2, no. 1, p. 011005, 2010.

[10] P. Grosch and F. Thomas, "Geometric path planning without maneuvers for nonholonomic parallel orienting robots," *IEEE Robotics and Automation Letters*, vol. 1, no. 2, pp. 1066–1072, 2016.

[11] M. Callegari, M. Battistelli, and R. Di Gregorio, "Design of a non-holonomic spherical wrist," *Journal of Intelligent & Robotic Systems*, vol. 81, no. 2, pp. 181–194, 2016.

[12] Z. Gao, L. Zeng, B. He, T. Luo, and P. Zhang, "Type synthesis of non-holonomic spherical constraint underactuated parallel robotics," *Acta Astronautica*, vol. 152, pp. 509–520, 2018.

[13] P. Grosch and F. Thomas, *Parallel Robots with Unconventional Joints: Kinematics and Motion Planning*, ser. Parallel Robots: Theory and Applications. Cham: Springer International Publishing, 2019.

[14] R. Brockett, "Asymptotic stability and feedback stabilization," in *Differential Geomettic Control Theory*, R. W. Brockett, R. S. Millman, and H. J. Sussmann, Eds. Boston: Birkhauser, 1983, pp. 181–191.

[15] H. Sira-Ramírez and S. K. Agrawal, *Differentially Flat Systems*. CRC Press, 2004.

[16] M. Fliess, J. Lévine, P. Martin, and P. Rouchon, "Flatness and defect of non-linear systems: introductory theory and examples," *International Journal of Control*, vol. 61, no. 6, p. 1327–1361, 1995.

[17] ——, "A Lie-Backlund approach to equivalence and flatness of nonlinear systems," *IEEE Transactions on Automatic Control*, vol. 44, no. 5, p. 922–937, 1999.

[18] M. A. Belabbas and S. Liu, "New method for motion planning for non-holonomic systems using partial differential equations," in *2017 American Control Conference (ACC)*. Seattle, WA, USA: IEEE, 2017, pp. 4189–4194.

[19] S. Zeng, "On the geometric construction of a stabilizing time-invariant state feedback controller for the nonholonomic integrator," *Automatica*, vol. 136, p. 110073, 2022.

[20] W. He, Y. Huang, and S. Zeng, "Motion planning with homotopy class constraints via the auxiliary energy reduction technique," in *2022 American Control Conference (ACC)*. Atlanta, GA, USA: IEEE, 2022, pp. 4933–4938.

[21] R. M. Murray and S. S. Sastry, "Nonholonomic motion planning: steering using sinusoids," *IEEE Transactions on Automatic Control*, vol. 38, no. 5, pp. 700–716, 1993.

[22] L. E. Dubins, "On curves of minimal length with a constraint on average curvature, and with prescribed initial and terminal positions and tangents," *American Journal of Mathematics*, vol. 79, no. 3, pp. 497–516, 1957.

[23] J. Reeds and L. Shepp, "Optimal paths for a car that goes both forwards and backwards," *Pacific Journal of Mathematics*, vol. 145, no. 2, pp. 367–393, 1990.

[24] F. Lamiraux and J.-P. Lammond, "Smooth motion planning for car-like vehicles," *IEEE Transactions on Robotics and Automation*, vol. 17, no. 4, p. 498–501, 2001.

[25] S. Sarabandi and F. Thomas, "Approximating displacements in $\mathbb{R}^3$ by rotations in $\mathbb{R}^4$ and its application to pointcloud registration," *IEEE Transactions on Robotics*, vol. 38, no. 4, p. 2652–2664, 2022.

[26] P. Martin and P. Rouchon, "Any (controllable) driftless system with m inputs and $m+2$ states is flat," in *Pro-*

ceedings of 1995 34th IEEE Conference on Decision and Control, vol. 3. New Orleans, LA, USA: IEEE, 1995, pp. 2886–2891.

[27] S.-J. Li and W. Respondek, "Flat outputs of two-input driftless control systems," *ESAIM: Control, Optimisation and Calculus of Variations*, vol. 18, no. 3, pp. 774–798, 2012.

[28] M. P. Hennessey, "Visualizing the motion of a unicycles on a sphere," *International Journal of Modelling and Simulation*, vol. 26, no. 1, pp. 69–79, 2006.

[29] J.-P. Laumond, S. Sekhavat, and F. Lamiraux, *Guidelines in nonholonomic motion planning*. New York: Springer-Verlag, 1998.

[30] J. R. Wertz, *Spacecraft Attitude Determination and Control*, ser. Astrophysics and Space Science Library. Dordrecht: Springer Netherlands, 1978, vol. 73.

[31] B. Graf, "Quaternions and dynamics," https://arxiv.org/pdf/0811.2889.pdf, accessed: 2010-09-30.

[32] R. W. Farebrother, J. Groß, and S.-O. Troschke, "Matrix representation of quaternions," *Linear Algebra and its Applications*, vol. 362, p. 251–255, 2003.

[33] G. S. Chirikjian and A. B. Kyatkin, *Engineering Applications of Noncommutative Harmonic Analysis with Emphasis on Rotation and Motion Groups*. CRC Press, 2001.

[34] M.-Y. Wu, "A new method of computing the state transition matrix of linear time-varying systems," in *Proceedings of the IEEE International Symposium on Circuits ans System*, 1974.

[35] ——, "An extension of "a new method of computing the state transition matrix of linear time-varying systems"," *IEEE Transactions on Automatic Control*, vol. 19, no. 5, p. 619–620, 1974.

[36] ——, "Some new results in linear time-varying systems," *IEEE Transactions on Automatic Control*, vol. 20, no. 1, p. 159–161, 1975.

[37] M.-Y. Wu, I. M. Horowitz, and J. C. Dennison, "On solution, stability and transformation of linear time-varying systems," *International Journal of Control*, vol. 22, no. 2, p. 169–180, 1975.

[38] J. Watkins and S. Yurkovich, *Calculation of the State Transition Matrix for Linear Time Varying Systems*. Boston, MA: Birkhäuser Boston, 1993, pp. 157–166.

[39] G. Marsaglia, "Choosing a point from the surface of a sphere," *The Annals of Mathematical Statistics*, vol. 43, no. 2, p. 645–646, 1972.

[40] H. Choset, *Principles of Robot Motion: Theory, Algorithms, and Implementation*, ser. Intelligent Robotics and Autonomous Agents. Cambridge, Mass: MIT Press, 2005.

[41] S. M. LaValle, *Planning Algorithms*. Cambridge, New York: Cambridge University Press, 2006.

Federico Thomas earned his B.Sc. in Telecommunications Engineering in 1984 and his Ph.D. (with honors) in Computer Science in 1988, both from the Technical University of Catalonia (UPC) in Spain. He has held distinguished visiting scholar positions at the University of Massachusetts (1991-1992) and Oxford University (1999-2000). Additionally, he served as an invited professor at the Institut de Recherche en Communications et Cybernétique de Nantes (IRCCyN) in 2009 and at the Department of Mechanical Engineering at the University of Ferrara in 2010.

Since 1990, Prof. Thomas has been a Research Scientist at the Institut de Robòtica i Informàtica Industrial, a joint institution of the Spanish High Council for Scientific Research (CSIC) and UPC, where he also held the position of director from 2006 to 2008. Additionally, he is a faculty member at the Institute of Mathematics at UPC-BarcelonaTech and an associate professor in the Mathematics Department at UPC since 2022.

Prof. Thomas has served as an associate editor for both IEEE Transactions on Robotics (TRO) and the ASME Journal of Robotics. He has authored approximately 200 papers in journals and conferences, primarily focusing on the theoretical aspects of robotics. His current research interests include Distance Geometry and Clifford Algebras, particularly their applications to robot kinematics.

Jaume Franch earned his B.Sc. in Mathematics from Universitat de Barcelona (UB) in 1992, and his PhD in Mathematics from Technical University of Catalonia (UPC) in 1999.

Since 2002, he has been an Associate Professor at UPC, where he served as Dean of the School of Mathematics and Statistics from 2015 to 2023. He has also been a visiting scholar at University of Delaware and Columbia University. His research focuses on nonlinear control and its applications to mechanical systems, particularly in Robotics.